AMERICAN SOCIETY FOR MICROBIOLOGY | Journal of Virology®

PATHOGENESIS AND IMMUNITY

Zika Virus Infection Induced Apoptosis by Modulating the Recruitment and Activation of Proapoptotic Protein Bax

Xiaodong Han,[a] Jiuqiang Wang,[d] Yang Yang,[b] Shuxiang Qu,[a] Fang Wan,[a] Ziyi Zhang,[a] Ruigang Wang,[a] Guojing Li,[a] Haolong Cong[b,c]

[a]College of Life Sciences, Inner Mongolia Agriculture University, Hohhot, People's Republic of China
[b]Chinese Academy of Inspection and Quarantine, Beijing, People's Republic of China
[c]Center for Molecular Virology, CAS Key Laboratory of Pathogenic Microbiology and Immunology, Institute of Microbiology, Chinese Academy of Sciences, Beijing, People's Republic of China
[d]State Key Laboratory of Membrane Biology, Institute of Zoology, Chinese Academy of Sciences, Beijing, People's Republic of China

Xiaodong Han, Haolong Cong, and Jiuqiang Wang contributed equally to this work. Author order was determined both alphabetically and in order of increasing seniority.

ABSTRACT Zika virus (ZIKV) infection is associated with microcephaly in newborns and serious neurological complications in adults. Apoptosis of neural progenitor cells induced by ZIKV infection is believed to be a main reason for ZIKV infection-related microcephaly. However, the detailed mechanism of ZIKV infection-induced apoptosis remains to be elucidated. In this report, ZIKV infection induced the conformational activation of the proapoptotic protein Bax, with subsequent formation of oligomers of Bax in the mitochondria. Cell apoptosis was reduced significantly in SY5Y cells subjected to Bax knockdown. Additionally, while decreasing Bax expression inhibited the release of cytochrome *c* (Cyt c) from the mitochondria and reduced the rate of loss of mitochondrial membrane potential induced by ZIKV infection, silencing Bak, caspase-8, and/or caspase-10 expression did not. Mitochondria isolated from the untreated ZIKV-infected cells displayed Bax-binding ability and the subsequent release of Cyt c. This study also indicated that the NS4B protein of ZIKV recruited Bax to the mitochondria and induced Bax conformational activation. The overexpressed NS4B was localized to the mitochondria and induced cell apoptosis by activating the proapoptotic protein Bax. All the above results indicated that ZIKV infection directly affected the mitochondrial apoptotic pathway by modulating the recruitment and activation of Bax.

IMPORTANCE Since the large outbreaks that occurred in the Pacific Islands and Latin America in 2013, Zika virus has been confirmed a neuroteratogenic pathogen and causative agent of microcephaly and other developmental anomalies of the central nervous system in children born to infected mothers. As apoptosis is widespread throughout the whole brain, studies in animal models have reinforced the link between microcephaly caused by ZIKV infection and neural progenitor cell (NPC) apoptosis. Currently, the detailed mechanism of ZIKV infection-induced apoptosis still remains to be elucidated. Here, we first demonstrate that ZIKV infection activated the classic signs of mitochondrial apoptotic pathway by modulating the recruitment and activation of Bax. ZIKV NS4B represents a novel viral apoptotic protein that can modulate the recruitment and activation of Bax and trigger the apoptotic program. This is a new insight into understanding the interplay between apoptosis and ZIKV infection.

KEYWORDS NS4B, Zika virus, microcephaly, mitochondrial apoptotic pathway, proapoptotic protein Bax

Zika virus (ZIKV) is an enveloped, single-stranded RNA virus in the *Flaviviridae* family that was first identified in rhesus monkeys in the Zika Forest in Uganda in 1947 (1).

Citation Han X, Wang J, Yang Y, Qu S, Wan F, Zhang Z, Wang R, Li G, Cong H. 2021. Zika virus infection induced apoptosis by modulating the recruitment and activation of proapoptotic protein Bax. J Virol 95:e01445-20. https://doi.org/10.1128/JVI.01445-20.

Editor Rebecca Ellis Dutch, University of Kentucky College of Medicine

Address correspondence to Haolong Cong, conghaolong@hotmail.com.

Received 18 July 2020
Accepted 15 January 2021
Accepted manuscript posted online 3 February 2021
Published 25 March 2021

Transmitted by the *Aedes* mosquito vector, ZIKV spread at an alarming rate and posed serious threats with outbreaks in Africa, the Pacific Islands, the Americas, and Southeast Asia (2). Not until the large outbreaks that occurred in the Pacific Islands and Latin America had the relationship between ZIKV and fever, rash, congenital microcephaly, and the rarer Guillain-Barre syndrome been identified (3–5). Recent reports further confirmed that ZIKV is a neuroteratogenic pathogen and is the causative agent of microcephaly and other developmental anomalies of the central nervous system (CNS) in children born to infected mothers (6–8). It is worth noting that the ZIKV African lineages are spreading in Brazil, one which was isolated from *Aedes albopictus* mosquito species and the other which was isolated from *Alouatta guariba*, a monkey species (9).

Microcephaly is by far the most severe, irreversible complication, resulting in a small cerebral cortex upon ZIKV infection. As the cerebral cortex develops mainly during the first trimester of pregnancy (10), ZIKV infection in pregnant women during this period is more likely to affect the CNS (11). Multiple reports on ZIKV infection, transmission, and possible mechanism of microcephaly at the molecular and biological levels had been published. They showed that ZIKV was transmitted from the infected mother to the fetus by crossing the placental barrier where the susceptible placental macrophages (Hofbauer cells) and cytotrophoblasts might facilitate virus entry (12, 13). ZIKV entry into the neural progenitor cells (NPCs) relied on the binding of the virus's protein E to the cell receptor and the formation of endosome (14). Subsequently, ZIKV replication activated the TLR3 receptors which mediated the regulation of genes associated with immune response, cell cycle, differentiation, and apoptosis in NPCs, resulting in neurological malformations (15, 16).

Studies in animal models also reinforced the link between microcephaly caused by ZIKV infection and NPC apoptosis. The brain mass of a wild-type mouse decreased significantly after only 4 days post ZIKV infection and displayed widespread apoptosis throughout the brain, with the occipital cortex and hippocampus having particularly robust apoptosis phenotype (17). The induction of apoptotic cell death in human NPCs by ZIKV infection was demonstrated by the activation of caspases 3/7, 8, and 9 and by ultrastructural and flow cytometry analyses (18). Furthermore, ZIKV infection-induced cell death could be prevented by incubating the cells with a pan-caspase inhibitor, thus implying that the apoptosis of NPCs induced by ZIKV infection contributed to microcephaly.

As a highly regulated form of programmed cell death, apoptosis can be triggered by two distinct signaling pathways: the death receptor pathway, which is initiated by the activation of cell death receptors, and the mitochondrial pathway that needs the disruption of the mitochondrial transmembrane potential (MMP), which usually involves a variety of pro- and antiapoptotic proteins of the Bcl-2 family (19–22). The proapoptotic Bcl-2 proteins Bak and Bax are required for the induction of apoptosis via the mitochondrial pathway (23). In most cells, Bax is normally localized in the cytosol or loosely associated with the outer mitochondrial membrane (OMM), whereas Bak is mostly localized in the OMM and remains inactive in nonapoptotic cells (24). Following cytotoxic stimulation, Bax undergoes a series of conformational changes which leads to its integration into the mitochondrial membranes and eventually induces apoptosis (25, 26). Upon activation, Bak is released from the antiapoptotic proteins and activates caspase-9 and the downstream death programs (27).

It was reported that ZIKV infection led to $Sox2^+$ cells apoptosis through activation of caspases 3, 8, and 9 and induced mitochondrial apoptosis in human lung epithelial A549 cells through activation of caspases 3 and 9 (28). In this study, we demonstrated that ZIKV infection activates the classic signs of the mitochondrial apoptotic pathway by directly altering Bax conformation and triggering its homo-oligomerization and redistribution from the cytosol to mitochondria. ZIKV NS4B represents a novel viral apoptotic protein that can modulate the recruitment and activation of Bax and trigger the apoptotic program. This is a new insight into understanding of the interplay between apoptosis and the ZIKV infection.

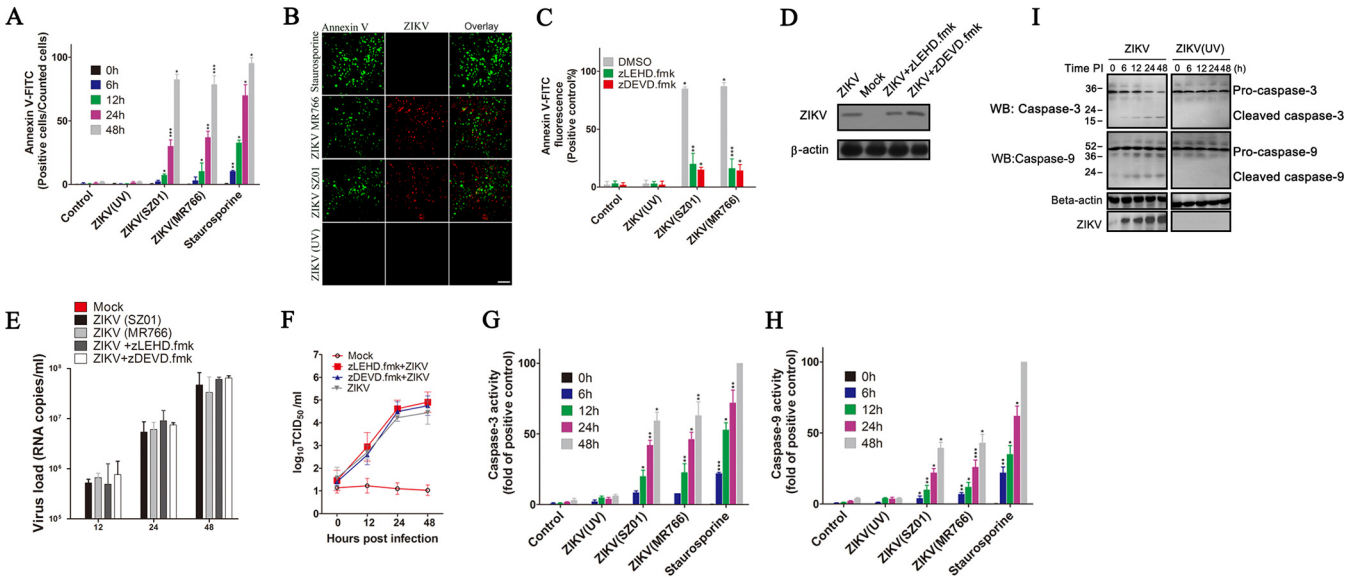

FIG 1 Activation of the mitochondrial apoptotic pathway with ZIKV infection. (A) Percentage of Annexin V-FITC positive cells at 0, 6, 12, 24, and 48 hpi. SY5Y cells were infected with ZIKV SZ01, ZIKV MR766, or ZIKV (UV) at an MOI of 1. Cells were then harvested at the indicated times, stained with Annexin V-FITC, and analyzed by flow cytometry. Control: cells with no virus infection. Staurosporine: cells treated with staurosporine (30 nM). (B) Detection of ZIKV infection-induced cell apoptosis by fluorescence microscopy. SY5Y cells were infected with ZIKV or ZIKV (UV) at an MOI of 1. Cells were stained with Annexin V-FITC (green) and ZIKV-specific antibody (red) at 48 hpi and then analyzed by fluorescence microscopy. (C) The effects of caspase inhibitors on cell apoptosis induced by ZIKV infection. Cells were infected with virus for 1 h at an MOI of 1. After washing three times with PBS, cells were treated with zDEVD.fmk (25 μM), zLEHD.fmk (15 μM), or dimethyl sulfoxide (DMSO) for another 48 h. The cells were harvested and stained with Annexin V-FITC and analyzed by flow cytometry. Control: cells with no virus infection. (D) Western blot showing the effect of caspase inhibitors on ZIKV-E protein. SY5Y cells were infected with ZIKV and then treated with zDEVD.fmk or zLEHD.fmk for another 48 h. Cell lysates were immunoblotted with antibody to ZIKV-E or to beta-actin (internal control). Mock: cells with no ZIKV infection. (E) Quantitative real-time PCR showing the effect of caspase inhibitors on RNA levels of ZIKV. RNA levels were performed at 12, 24, and 48 h after treatment with zDEVD.fmk or zLEHD.fmk. Mock: cells with no ZIKV infection. (F) The effect of caspase inhibitors on virus titers of ZIKV. Viral titers in cell supernatants were determined by 50% tissue culture infective dose ($TCID_{50}$) experiment in Vero-E6 cells. Mock, Vero- E6 cells with no ZIKV infection. $TCID_{50}$: 50% tissue culture infective dose. (G and H) Analysis of caspase-3 and caspase-9 activity in the separated cytoplasmic fractions of SY5Y cells with ZIKV infection. Caspase-3 and caspase-9 activity was measured by caspase-3 activity assay and caspase-9 activity assay as described in Materials and Methods. (I) Western blot of the activation of caspase-3 and caspase-9 in ZIKV-infected cells. Cells were infected with ZIKV or ZIKV (UV) at an MOI of 2 PFU $cell^{-1}$. Cells were harvested at 0, 6, 12, 24, and 48 hpi and then analyzed with pro- and cleaved-caspase-3/9 antibody. Data are from three independent experiments and the results are presented as mean ± standard error of the mean (SEM). ** indicates a significant difference at *P* values of 0.02 compared to the control; * indicates a significant difference at *P* values of 0.05 compared to the control.

RESULTS

Activation of the mitochondrial apoptotic pathway in ZIKV-infected cells. To determine if ZIKV infection could induce apoptosis in SY5Y cells, we measured the formation of apoptotic cells by using the Annexin V-FITC apoptosis staining/detection kit at the indicated times postinfection. SY5Y cells were infected with ZIKV strains MR766, SZ01, and ZIKV (UV) (strain MR766 was inactivated by UV). The percentage of Annexin V-FITC positive cells increased from 12% at 12 hours postinfection (hpi) to 86% at 48 hpi in ZIKV-infected cells, while no more than 3% of cells infected with ZIKV (UV) or control displayed Annexin V fluorescence intensity at 48 hpi. Comparatively, ZIKV infection exhibited the same ability to induce cell apoptosis as staurosporine (an apoptosis inducer by activating caspase-3), which indicated that ZIKV infection could initiate SY5Y cells apoptosis (Fig. 1A and B).

To determine if caspases are crucial to ZIKV infection-induced apoptosis in SY5Y cells, we examined the effects of the caspase inhibitors zDEVD.fmk and zLEHD.fmk. zDEVD.fmk is a wide-spectrum caspase inhibitor that irreversibly inhibits caspase-3 as well as other proteases, including caspase-6, caspase-8, and caspase-10, and zLEHD. fmk is an irreversible inhibitor of caspase-9. As shown in Fig. 1C, infection with ZIKV strains MR766 and SZ01 could induce more than 80% cells apoptosis at 48 hpi. When ZIKV-infected cells were treated with zDEVD.fmk or zLEHD.fmk, the percentage of activation of cell apoptosis was suppressed at ~15% to 25%. To detect whether those caspase inhibitors influence the gene expression of ZIKV, we measured ZIKV-E protein, ZIKV RNA levels, and viral titers in cells that were treated by caspase inhibitors. Results

indicated that the inhibitors have no obvious effects on viral gene expression at the indicated concentration (Fig. 1D to F) in our study. The above results indicated that the apoptosis was sharply inhibited by caspase inhibitors, and the formation of apoptotic cells induced by ZIKV infection was dependent on caspase activation.

The induction of the mitochondrial apoptotic pathway during ZIKV infection was further tested by monitoring the activation of caspase-3 or caspase-9 in ZIKV-infected cells. The activity of the activated caspase-3 and activated caspase-9 in the separated cytoplasm was quantified using caspase-3/9 activity assay kit. Results showed that cells treated with staurosporine or infected with ZIKV displayed a significant increase of caspase-3 or caspase-9 activity (56% and 58% at 48 hpi, respectively), while only a small amount of caspase-3 or caspase-9 activation was detected in ZIKV (UV)- or mock-infected cells (Fig. 1G and H). Western blotting showed that activation of both caspase-3 and caspase-9 increased gradually with the extension of infection time. From 6 h postinfection, lower molecular weight bands representing the active forms of caspase-3 and caspase-9 could be detected obviously in ZIKV-infected cells (Fig. 1I). This implied that ZIKV infection resulted in the proteolytic processing of inactive caspase-3 and caspase-9 zymogens into their respective activated fragments. In contrast, neither caspase-3 nor caspase-9 activation was observed in cells infected with ZIKV (UV).

Induction, translocation, and activation of Bax in ZIKV-infected cells. The above results indicated that ZIKV infection activated caspase-3 and caspase-9. Therefore, we inquired whether ZIKV infection acted by modulating members of the Bcl-2 family which tightly regulated the mitochondria checkpoint in apoptotic cells. Since the active forms of both Bax and Bak are responsible for destabilizing the mitochondrial membrane by exposing their N-terminal epitope (29), we first conducted flow cytometry analysis to detect the active form of Bak and Bax in ZIKV-infected cells using conformation-specific anti-Bak and anti-Bax6A7 antibody that specially recognizes the exposed N terminus. The results showed an obvious increase in Bak fluorescence intensity only in cells treated with staurosporine but not in cells infected with ZIKV or ZIKV (UV) (Fig. 2A), indicating that ZIKV infection did not activate Bak. Cells that were infected with ZIKV showed an obvious Bax6A7 fluorescence, indicating that ZIKV infection induced the N-terminal exposure of Bax.

The activated Bax was further confirmed by immunofluorescence study using anti-Bax6A7 antibody (30). The activated Bax signals were detected only in cells infected with ZIKV or treated with staurosporine, which colocalized with ZIKV signals very well, which indicated that ZIKV infection induced activation of Bax (Fig. 2B). The results of cell counting showed that there were on average 87% Bax6A7 positive cells and 85% ZIKV/Bax6A7 merged cells among ZIKV-infected cells, indicating that the Bax6A7 positive cells correlated with ZIKV positive cells (Fig. 2C). The coimmunoprecipitation assays also showed that activated Bax can be precipitated from cells infected with ZIKV or treated with staurosporine, not from cells infected with ZIKV (UV) and mock, which confirmed the Bax activation during ZIKV infection (Fig. 2D).

To determine if ZIKV infection does induce Bax translocation into mitochondria and consequently results in Bax conformational change, the mitochondrial and cytosolic fractions from ZIKV-infected, ZIKV (UV)-infected, staurosporine-treated, and control cells were separated by centrifugation. The distribution of Bax in the mitochondrial and cytosolic fractions was analyzed by immunoblotting with an anti-BaxNT antibody, and the Cox IV, beta-actin, and ZIKV-E protein were also measured, respectively. As shown in Fig. 2E, in mitochondrial fractions, a clear band of Bax was observed only in the ZIKV-infected and staurosporine-treated cells. In cytosolic fractions, a lot of Bax was detected in control and ZIKV (UV)-infected cells, and a small amount of Bax was detected in ZIKV-infected and staurosporine-treated cells. The above results indicated that ZIKV infection led to the translocation of Bax from the cytoplasm to mitochondria.

Since only the activated form of Bax is oligomerized (31), high molecular weight Bax complexes formed in mitochondria during ZIKV infection were fixed by chemically cross-linking with bis-maleimidohexane (BMH) and detected by Western blotting. In

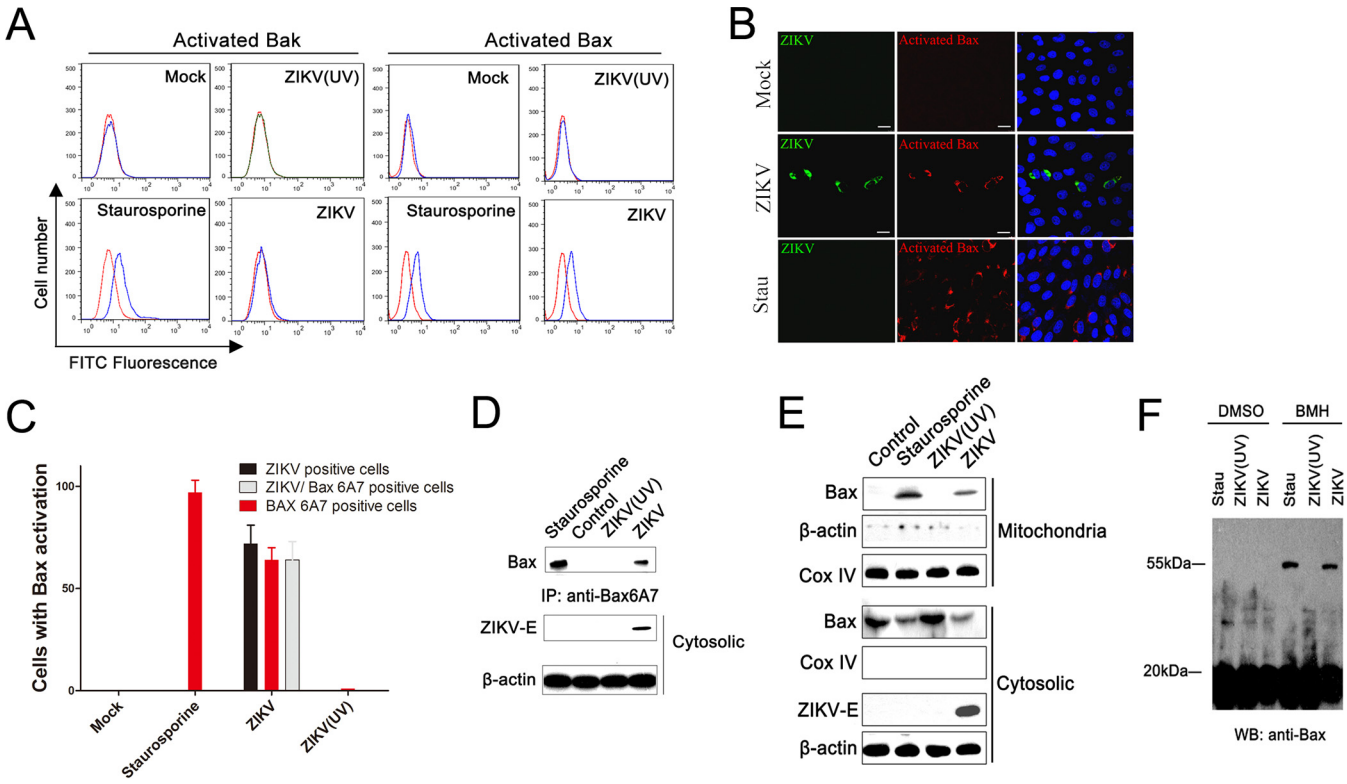

FIG 2 Activation of proapoptotic protein Bax in ZIKV-infected cells. (A) Flow cytometry analysis of the activation of Bak and Bax in SY5Y cells infected with ZIKV or ZIKV (UV). At 24 hpi, the activated Bak and Bax in cells were stained by a conformation-specific anti-Bak and anti-Bax6A7 antibody. Staurosporine: cells treated with staurosporine (30 nM) for 12 h. Mock: cells with no ZIKV infection. (B) Immunofluorescence analysis of activated Bax and ZIKV-E protein in cells infected with ZIKV. LLC-MK_2 cells were infected with ZIKV (SZ01) for 12 h, fixed with 4% paraformaldehyde, and then stained with antibody to ZIKV-E and activated Bax. Stau: cells treated with staurosporine. (C) SY5Y cells were infected with ZIKV (MR766) for 24 h and fixed with 4% paraformaldehyde. The ratio of ZIKV positive cells, Bax6A7 positive cells, and both ZIKV and Bax6A7 positive cells (per 100 cells) was determined by immunofluorescence analysis. Mock: cells with no ZIKV infection. Data are from three independent experiments and the results are presented as mean ± SEM. (D) Western blot of the activated Bax in cells infected with ZIKV. LLC-MK_2 cells were infected with ZIKV as described above and then lysed. Cell lysates were immunoblotted with antibody to ZIKV-E or to β-actin and immunoprecipitated with anti-Bax6A7 antibody. Control: cells with no ZIKV infection. (E) Western blot of Bax distribution in cytosolic and mitochondrial fractions of LLC-MK_2 cells infected with ZIKV. At 12 hpi, the cytosolic and mitochondrial fractions were separated and immunoblotted with antibody to ZIKV-E, Cox IV, β-actin, Bax, and activated Bax. Control: cells with no ZIKV infection. (F) Western blot of the homo-oligomerization of Bax induced by ZIKV infection. SY5Y cells were infected with ZIKV, and mitochondrial fractions were separated by centrifugation. After cross-linking with BMH or DMSO, equal amounts of the mitochondrial fractions were immunoblotted with anti-Bax antibody. DMSO was used to dissolve the BMH. Stau: cells treated with staurosporine (30 nM) for 12 h.

the absence of BMH, Bax from both ZIKV- and ZIKV (UV)-infected cells, and staurosporine-treated cells, appeared at an approximately 20 kDa band. However, after BMH cross-linking, Bax formed dimer in both ZIKV-infected and staurosporine-treated cells but not in ZIKV (UV)-infected cells (Fig. 2F). The appearance of the intramolecular cross-linked Bax species in the purified mitochondria indicates that ZIKV infection could induce the activation of Bax and the formation of Bax oligomers.

To further investigate the apoptosis and Bax activation, the spleens from 7-week-old type I interferon (IFN) receptor α chain null mice (Ifnar1$^{-/-}$) infected with ZIKV for 5 days were collected and measured by immunofluorescence. At high levels of ZIKV infection signals in spleens, the cleaved-caspase-3 signals and activated Bax signals were detected obviously, while no activated Bax and only vaguely background cleaved-caspase-3 signals can be detected in spleens from uninfected mice (Fig. 3A). The obvious activated caspase-3 signals and activated Bax signals also could be detected in ZIKV-infected Ifnar1$^{-/-}$ fetal brain, whereas low levels of physiological apoptosis could be detected in uninfected fetuses. Moreover, both the activated caspase-3 signals and activated Bax signals from fetal brain or spleen merged with ZIKV-E signals very well (Fig. 3B). Cell counting experiments showed that there were in average 73% activated Bax cells, 71% activated caspase-3 cells, 66% ZIKV/activated Bax merged cells, and 65% ZIKV/activated caspase-3 merged cells among ZIKV-infected cells from spleen.

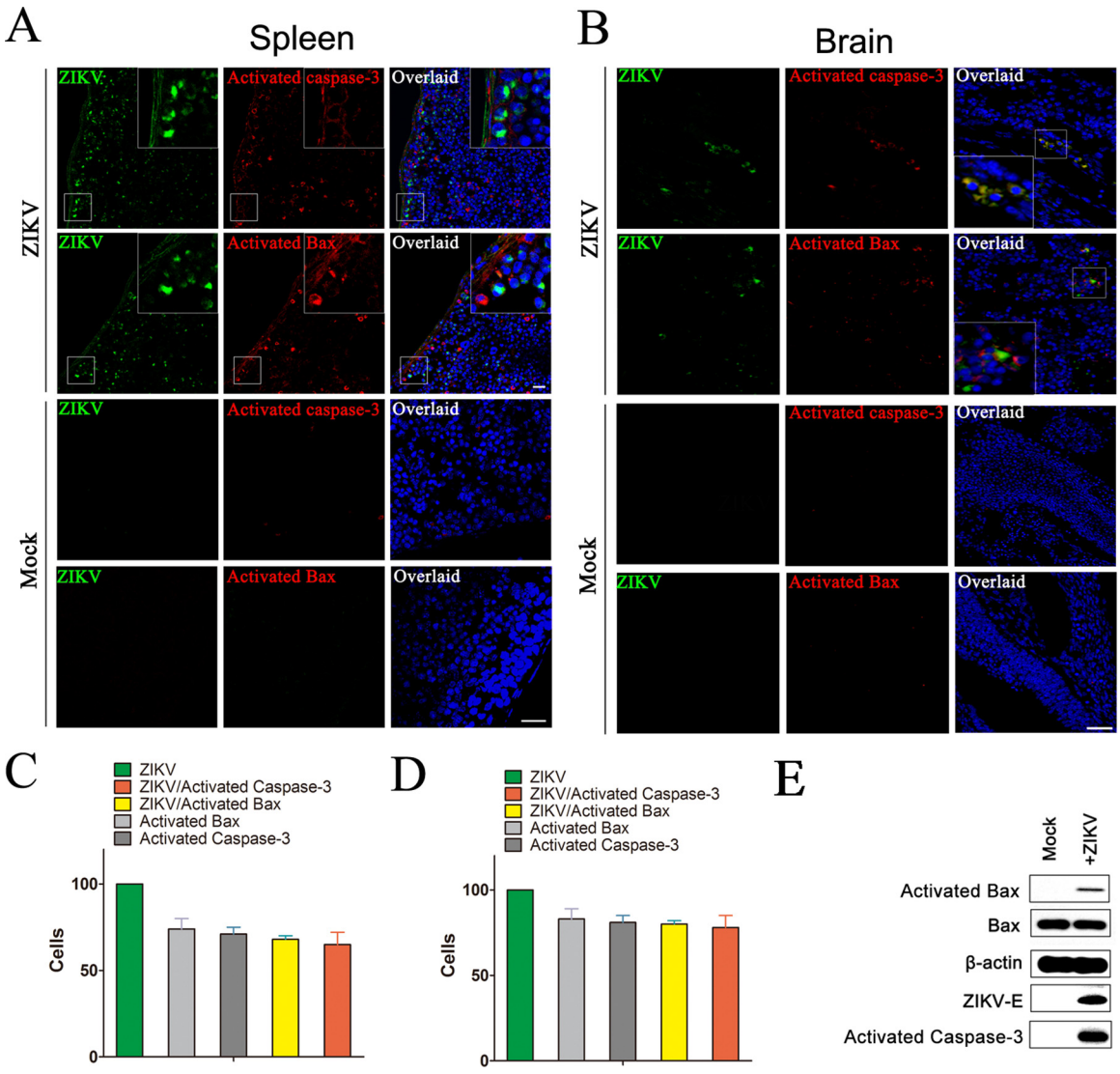

FIG 3 ZIKV infection is associated with evidence of apoptosis in mice spleen and the fetal brain. (A) Immunofluorescence analysis of the apoptosis in spleen of mice infected with ZIKV. Seven-week-old Ifnar1$^{-/-}$ mice were inoculated with 10^3 PFU of ZIKV via a subcutaneous route. After 5 days, mice were sacrificed and the spleens were collected for immunofluorescence analysis with ZIKV-E antibody (green), activated caspase-3 antibody (red), and activated Bax antibody (red). DAPI was colored blue. (B) Immunofluorescence analysis of the apoptosis in brain of fetal mice infected with ZIKV. Pregnant Ifnar1$^{-/-}$ mice (6 days post fertilization) were inoculated with 10^3 PFU of ZIKV via a subcutaneous route. After 7 days, the brain of fetal mice was collected for immunofluorescence analysis with antibody to ZIKV-E, activated Bax, or activated caspase-3. Mock: mice with no ZIKV infection. (C) The ratio of ZIKV positive cells, Bax6A7 positive cells, and both ZIKV and Bax6A7 positive cells in spleen of mice. (D) The ratio of ZIKV positive cells, Bax6A7 positive cells, and both ZIKV and Bax6A7 positive cells in brain of fetal mice. Data are from three independent experiments and the results are presented as mean ± SEM. (E) Western blot of the Bax, activated Bax, and activated caspase-3 in the brain of fetal mice infected with ZIKV. At 7 days postinfection, the brain of fetal mice was collected and homogenized and then immunoblotted with antibody to ZIKV-E, activated Bax, or activated caspase 3. Mock: mice with no ZIKV infection. ZIKV-E: Zika virus's protein E.

In addition, there are 83% activated Bax cells, 81% activated caspase-3 cells, 79% ZIKV/activated Bax merged cells, and 77% ZIKV/activated caspase-3 merged cells among ZIKV-infected cells from fetal brain, indicating that the activation of Bax and caspase-3 correlated with ZIKV infection (Fig. 3C and D). Western blotting also showed that the activated caspase-3 and activated Bax could be detected by cleaved-caspase-3 and Bax6A7 antibody in fetal brains homogenate with ZIKV infection (Fig. 3E). Those results indeed confirmed that ZIKV infection induces the activation of Bax.

Importance of Bax on apoptosis in ZIKV-infected cells. To determine the importance of Bax on ZIKV infection-induced apoptosis relative to other proteases, siRNA

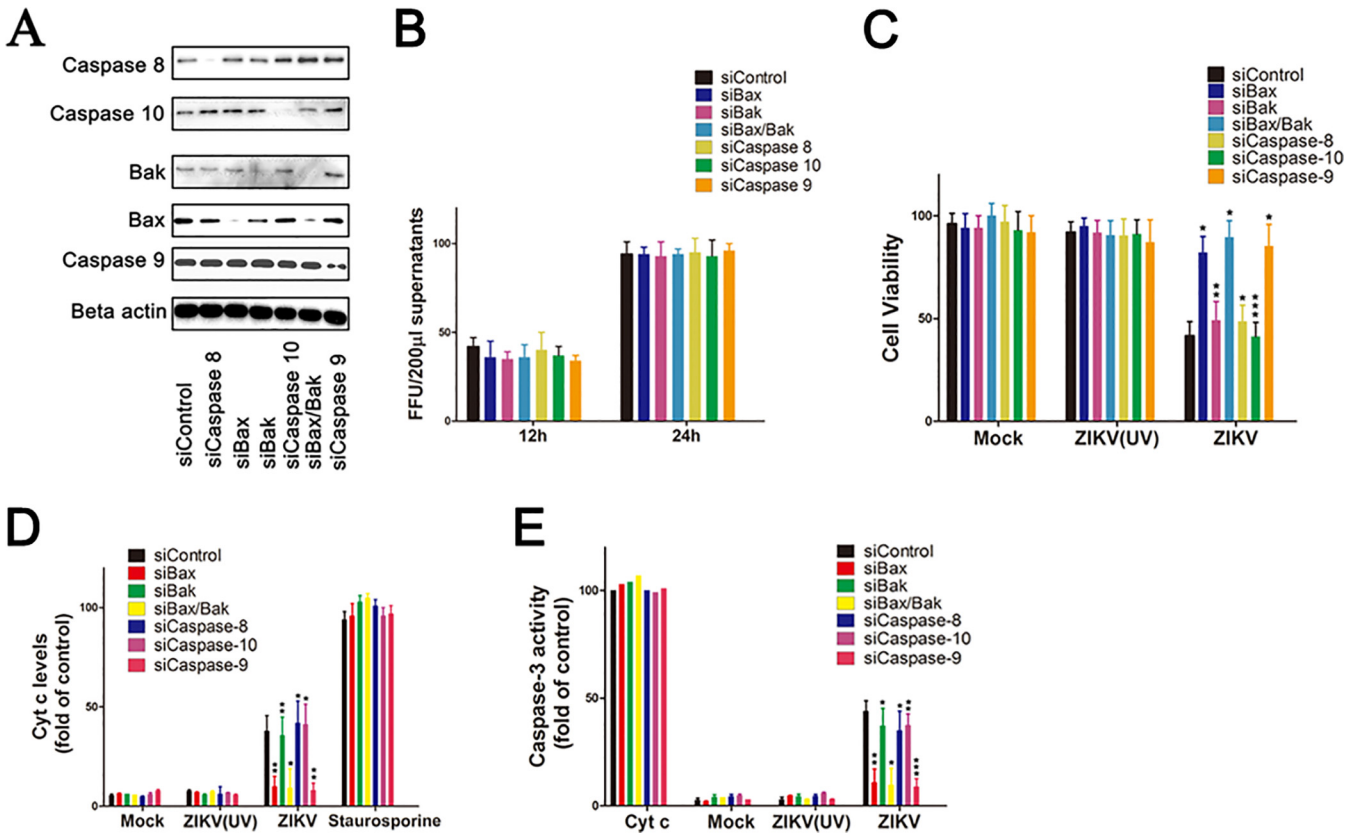

FIG 4 Impact of the downregulation of Bax, Bak, caspase-8, caspase-9, and caspase-10 expression on cell apoptosis induced by ZIKV infection. (A) Western blot of the specificity and effect of protein knockdown in siRNA-transfected cells. SY5Y cells were transfected with siRNA for 48 h and then cell lysates were prepared for immunoblot with antibody to Bak, Bax, beta-actin, caspase-8, caspase-9, and caspase-10. siControl: cells transfected with no targeting siRNA. siBax/Bak: cells transfected with both siBax and siBak. (B) ZIKV levels in the siRNA-transfected cells supernatants determined by immunofluorescence focus units assay analysis (FFU). SY5Y cells were transfected with siRNA targets to Bax, Bak, both Bax and Bak (Bax/Bak), caspase-8, caspase-9, and caspase-10. At 48 h posttransfection, cells were infected with ZIKV for another 12 h or 24 h. Cell supernatants were collected and subjected to FFU analysis with ZIKV-E antibody. siControl: cells transfected with no targeting siRNA. (C) Analysis of the impact of ZIKV infection on the viability of siRNA-transfected cells. Cells were transfected with siRNA as described above. At 48 h posttransfection, the cells were infected with ZIKV (MOI = 1) for 24 h and subjected to cell viability analysis by ELISA. Mock: uninfected cells. (D) Analysis of the impact of ZIKV infection on the release Cyt c in siRNA-transfected cells. The release of Cyt c in cytosolic fractions was determined as described in Materials and Methods. Staurosporine: siRNA-transfected cells treated with 30 nM staurosporine for 12 h. (E) Analysis of caspase-3 activity in cells after siRNA transfection and ZIKV infection. Caspase-3 activity was measured as described in Materials and Methods. Cyt c = cytosolic fractions of SY5Y cells incubated with Cyt c (10 μM). Data are from three independent experiments and the results are presented as mean ± SEM. ** indicates a significant difference at *P* values of 0.02 compared to the control; * indicates a significant difference at *P* values of 0.05 compared to the control.

knockdown experiments were performed. SY5Y cells were transfected with siRNA against Bax, Bak, both Bax and Bak (Bax/Bak), caspase-8, caspase-9, caspase-10, or nontargeting siRNA as a control. At 48 h posttransfection, cells were lysed and analyzed by Western blotting with the corresponding antibody. Results showed that the expression levels of caspase-8, caspase-9, and caspase-10 were reduced in corresponding siRNA-transfected cells compared to those in siControl. In addition, the expression levels of Bax and Bak were sharply decreased not only in siBax- and siBak-transfected cells but also in siBax/Bak-transfected cells (Fig. 4A). Cells were infected with ZIKV for another 12 or 24 h. The replication of ZIKV was monitored at 12 and 24 h after siRNA-transfected cells were immunoblotted with antibody against ZIKV-E protein. Results showed that knockdown of Bax, Bak, and caspase-8, -9, and -10 have no effect on ZIKV gene expression (Fig. 4B).

To analyze the impact of Bax, Bak, Bax/Bak, caspase-8, caspase-9, and caspase-10 knockdown on cell viability, the release of Cyt c, and caspase-3 activity, SY5Y cells were infected with ZIKV at 48 h posttransfection for all subsequent experiments. The cell viability was determined at 24 hpi. Results showed that ZIKV rapidly induced the decrease of cell viability in the siBak, siCaspase-8-, siCaspase-10-, and siControl-transfected cells,

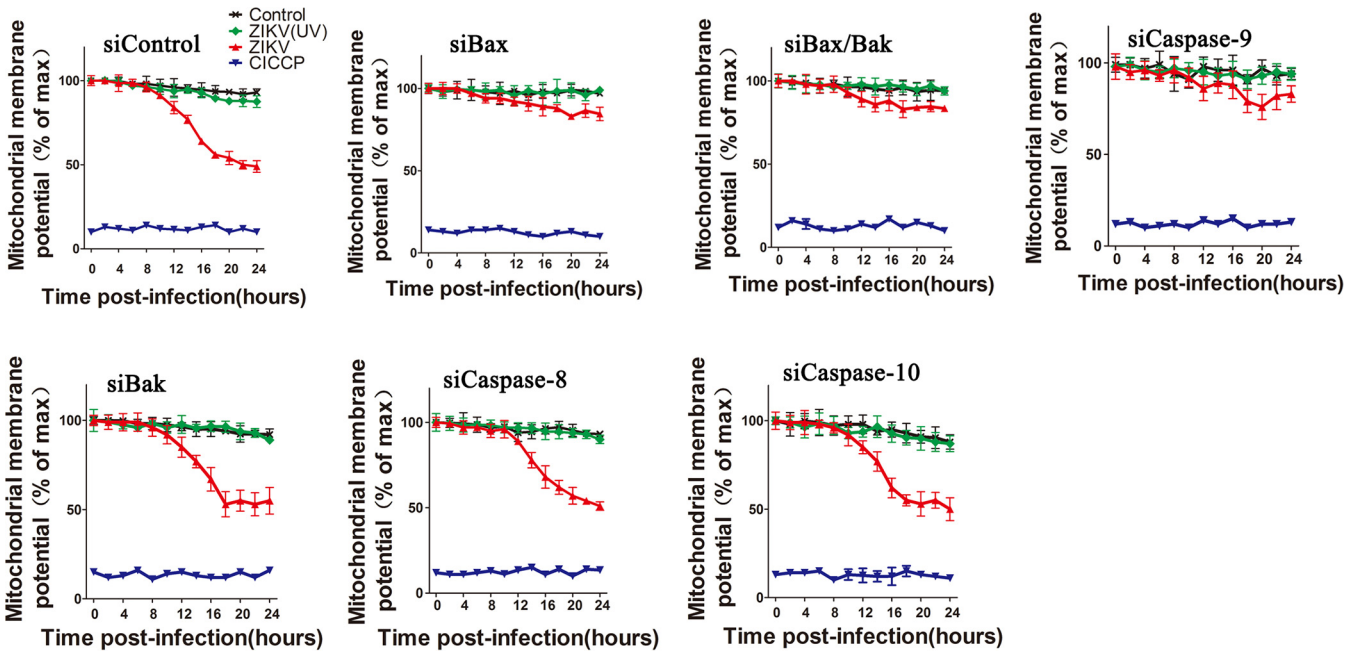

FIG 5 Flow cytometry analysis of the impact of Bax, Bak, caspase-8, caspase-9, and caspase-10 downregulation on inner mitochondrial membrane potential of ZIKV-infected cells. Cells were transfected with siRNAs as described above and infected with ZIKV. At 0, 4, 8, 12, 16, 20, and 24 hpi, cells were then stained with TMRE for 10 min at 37°C and subjected to flow cytometry analysis. CICCP, siRNA-transfected cells treated with carbonyl cyanide *m*-chlorophenyl hydrazine (10 μM). siControl: cells transfected with no targeting siRNA. Control: siRNA-transfected cells without ZIKV infection. siBax/Bak: cells transfected with both siBax and siBak. Data are from three independent experiments and the results are presented as mean ± SEM.

and the final cell death was more than 50% (Fig. 4C). However, the loss of cell viability induced by ZIKV infection was delayed in siBax-, siCaspase-9-, and siBak/Bax- transfected cells, with less than 10% of the loss of cell viability compared to 5% cell death infected with ZIKV (UV) and mock.

The release of Cyt c from mitochondria to the cytosol was detected in the cytosolic fractions. The results showed that the supernatants of ZIKV-infected cells transfected with siControl, siCaspase-8, siCaspase-10, and siBak all contained larger amounts of Cyt c, up to 45% more than the amount of Cyt c from the supernatants of cells treated with staurosporine. In addition, the Cyt c losses from the mitochondria of cells transfected with siBax, siBak/Bax, or siCaspase-9 were significantly attenuated, with no more Cyt c release than that of cells infected with ZIKV (UV) and mock (Fig. 4D).

The induction of apoptosis in ZIKV-infected cells was further confirmed by analysis of caspase-3 activity in the separated cytosolic fractions. The cytosolic fractions added with Cyt c were used as a positive control. Results showed that ZIKV-infected cells transfected with siControl, siCaspase-8, siCaspase-10, and siBak had higher levels of caspase-3 activity, up to 43% compared to 100% activated by Cyt c, while the cells transfected with siBax, siBak/Bax, or siCaspase-9 had no more than 13% caspase-3 activity. As expected, ZIKV (UV)- and mock-infected cells exhibited little or no caspase-3 activity (Fig. 4E).

The effect of ZIKV infection on the mitochondrial membrane potential was also studied by flow cytometry. Ionophore carbonyl cyanide *m*-chlorophenylhydrazone (CICCP) was used as a positive control. ZIKV-infected cells transfected with siCaspase-8, siCaspase-10, siBak, and siControl all showed a clear loss of the inner mitochondrial membrane potential (Fig. 5). In contrast, the ZIKV-infected cells transfected with siBax, siBak/Bax, or siCaspase-9 maintained a high level of tetramethylrhodamine ethyl ester (TMRE) fluorescence, indicating only a very small loss of inner mitochondrial membrane potential. As expected, both the control and ZIKV (UV)-infected cells maintained high levels of TMRE fluorescence.

All in all, the silencing of Bax and caspase-9 expressions inhibited caspase-3 activity

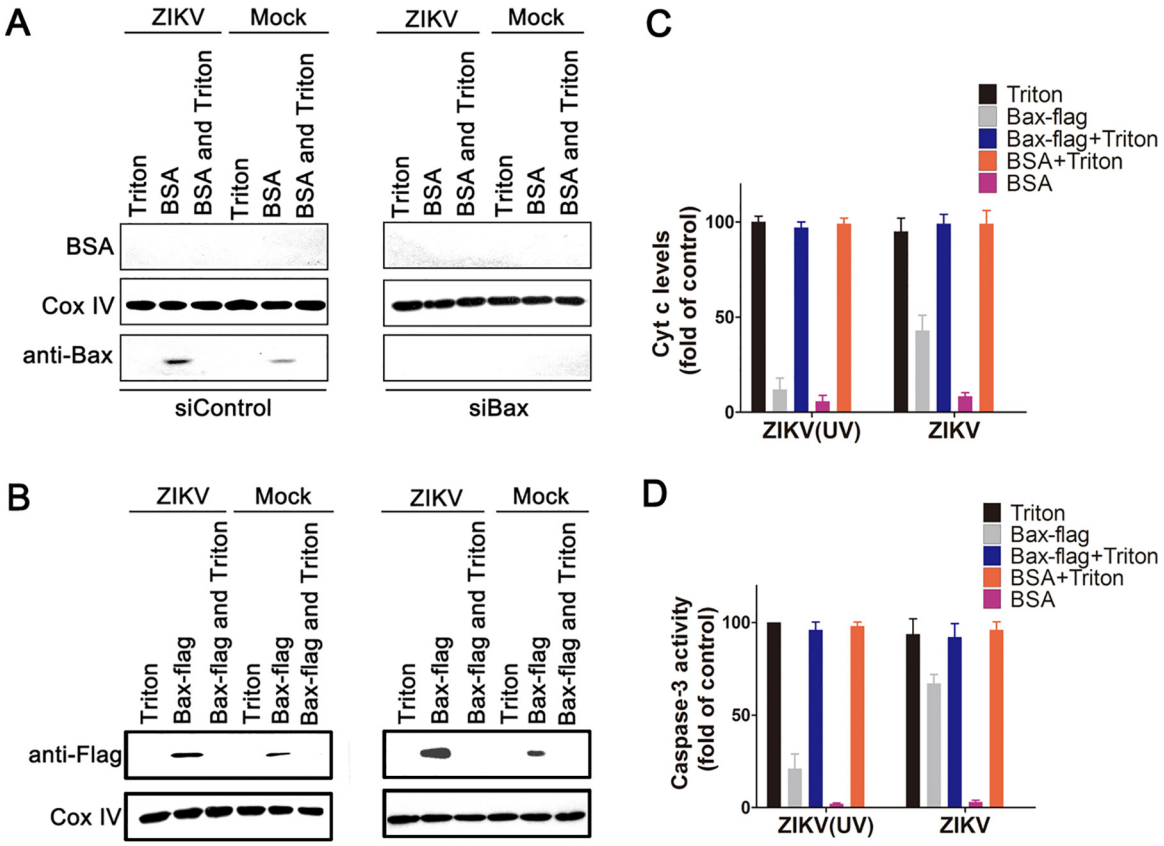

FIG 6 Mitochondrial fractions from ZIKV-infected cells induce recombinant Bax protein activation. (A) Western blot of the endogenous Bax in mitochondrial fractions of siBax-transfected cells. SY5Y cells were transfected with siBax for 48 h and then infected with ZIKV for another 24 h. The mitochondria were separated and incubated with 0.5 μM BSA or/and Triton X-100 (0.2% vol/vol) for 1 h. Then, the mitochondria were pelleted by centrifugation and immunoblotted with antibody to Bax, BSA, and Cox IV. siControl: cells transfected with no targeting siRNA. Triton: Triton X-100-treated mitochondria. BSA: BSA (0.5 μM)-treated mitochondria. BSA and Triton: mitochondria treated by BSA (0.5 μM) and Triton X-100 (0.2% vol/vol). (B) Western blot of the recruitment of exogenous Bax to mitochondria. The separated mitochondria were incubated with recombinant Bax or/and Triton X-100 at room temperature for 2 h. Then, the pelleted mitochondria were immunoblotted with antibody to Flag and Cox IV. siControl: cells transfected with siRNA that target to Bax. Bax-flag: Bax-flag (0.5 μM)-treated mitochondria. Bax-flag and Triton: mitochondria treated by Bax-flag (0.5 μM) and Triton X-100 (0.2% vol/vol). (C and D) The impact of exogenous Bax on Cyt c release and caspase-3 activity in isolated mitochondria from siBax-transfected cells with ZIKV infection. The separated mitochondria were incubated with BSA, Triton X-100, and an exogenous Bax for 1 h as above. The supernatants were then collected and subjected to Cyt c assay and caspase-3 activity assay. Data are from three independent experiments and the results are presented as mean ± SEM.

and the release of Cyt c from the mitochondria and reduced the rate and amount of cell death and mitochondrial membrane potential loss in ZIKV-infected cells. However, silencing Bak, caspase-8, or caspase-10 expression almost did not affect the apoptosis.

Isolated mitochondria from ZIKV-infected cells could induce the activation of recombinant Bax. As apoptosis induced by ZIKV infection was dependent on the activated Bax recruitment in mitochondria, we conducted experiments to further analyze how this occurs. First, SY5Y cells were transfected with siBax or siControl for 48 h and then infected with ZIKV or ZIKV (UV) for another 24 h. Bovine serum albumin (BSA) was used as a negative control. The mitochondria were separated and incubated with BSA, Triton X-100, and a recombinant Bax (Bax-Flag) for 1 h. The mitochondria were pelleted by centrifugation for Western blot, and the resulting supernatants were pooled for the assay of Cyt c release and caspase-3 activity.

The results showed that the endogenous Bax was depleted effectively by siBax regardless of ZIKV infection. Only in siControl-transfected mitochondria treated with BSA, a small amount of Bax can be detected, while the mitochondrial membrane was dissolved into supernatants by Triton X-100 (Fig. 6A). We also notice that the amount of Bax from mitochondria infected with ZIKV was larger than that from mitochondria

infected with ZIKV (UV). This is because the former is Bax-activated by ZIKV infection and the latter is the background Bax, which loosely associated with mitochondria membrane (Fig. 6A). A large amount of exogenous Bax-Flag can be detected at mitochondria membrane by ZIKV infection, while a small amount of Bax-Flag can be detected at ZIKV (UV)-infected mitochondria membrane. This difference caused by ZIKV infection was more obvious in siBax-transfected mitochondria membrane than in siControl-transfected cells, due to the knockdown of endogenous Bax (Fig. 6B).

The amounts of Cyt c were detected in the supernatant fractions of Bax-Flag-incubated mitochondria isolated from siBax-transfected cells. Results showed that 100% of Cyt c was detected in the supernatants from mitochondria treated with Triton X-100, regardless of ZIKV infection. However, without Triton X-100, the added Bax-Flag induced about 44% of the total Cyt c release from the mitochondria with ZIKV infection. In addition, only about 9% of Cyt c released from the mitochondria with ZIKV (UV) infection, which was equal to the amount of Cyt c released from BSA-incubated mitochondria with or without ZIKV infection (Fig. 6C).

To investigate if the Bax-Flag-treated mitochondria could release factors that induce the activation of DEVD-cleaving caspases, isolated mitochondria were incubated with Bax-Flag, BSA, or Triton X-100 for 1 h, followed by removal of the mitochondria by centrifugation and collection of the resulting supernatants (32). These supernatants were then added to the cytosolic fractions derived from SY5Y cells, and caspase-3 activity was measured 0.5 h later by spectrofluorimetric assays. These experiments showed that higher caspase-3 activity (100%) was detected from mitochondria sample treated with Triton X-100, while no more than 5% caspase-3 activity was detected from BSA treated mitochondria, regardless of ZIKV infection (Fig. 6D). The addition of supernatants derived from Bax-Flag-treated mitochondria with ZIKV (UV) infection only resulted in modest elevation (25%) in caspase-3 activity. However, supernatants from Bax-Flag-treated mitochondria with ZIKV infection caused a striking increase (75%) in caspase-3 activity (Fig. 6D). Altogether, these results suggest that ZIKV recruited Bax protein to mitochondria by directly modulating cell mitochondria.

Effect of Bcl-X_L on ZIKV infection-induced Bax activation and cell apoptosis. Bcl-X_L is known to form heterodimers with Bax, inhibiting its apoptotic effect (33). Thus, the impact of Bcl-X_L protein on cell apoptosis and activation of Bax induced by ZIKV infection were examined using SY5Y cells overexpressing Flag-Bcl-X_L. SY5Y cells that overexpressed bacterial alkaline phosphatase (BAP) were used as a control. Cell apoptosis was analyzed by Annexin V-FITC staining. As shown in Fig. 7A, in pCMV-BAP-transfected SY5Y cell line, 50% of cells infected with ZIKV (MR766 or SZ01) displayed Annexin V fluorescence intensity, compared to 100% of SY5Y-BAP cells treated with staurosporine. However, pCMV-Bcl-X_L-transfected SY5Y cells that were infected with ZIKV displayed a low Annexin V fluorescence intensity (about 15% when cells were transfected with 4 μg of pCMV-Bcl-X_L plasmid). The Annexin V fluorescence intensity in cells infected with ZIKV decreased obviously with the increasing amounts of pCMV-Bcl-X_L plasmid, indicating that Bcl-X_L inhibited the apoptosis induced by ZIKV infection.

The activation of Bax was further analyzed by coimmunoprecipitation assays using anti-Bax6A7 antibody. A large amount of activated Bax was precipitated detectably in staurosporine-treated and ZIKV-infected SY5Y-BAP cells (cells transfected with pCMV-BAP plasmid), but little or no activated Bax was detected in the SY5Y-Bcl-X_L cells (cells transfected with pCMV-Bcl-X_L plasmid). This indicated that the overexpressed Flag-Bcl-X_L efficiently inhibited the activation of Bax (Fig. 7B). The release of Cyt c from the mitochondria of SY5Y-Bcl-X_L cells was also investigated by Western blotting. Cyt c was detected in the cytoplasm fraction of SY5Y-BAP cells infected with ZIKV or treated with staurosporine but not in SY5Y-Bcl-X_L cells (Fig. 7B).

The loss of inner mitochondrial membrane potential was also analyzed in SY5Y-Bcl-X_L cells with ZIKV infection. CICCP was used as a positive control. As shown in Fig. 7C, ZIKV infection induced the loss of the inner mitochondrial membrane potential in SY5Y-BAP cells after 10 h postinfection. However, SY5Y-Bcl-X_L cells infected with ZIKV

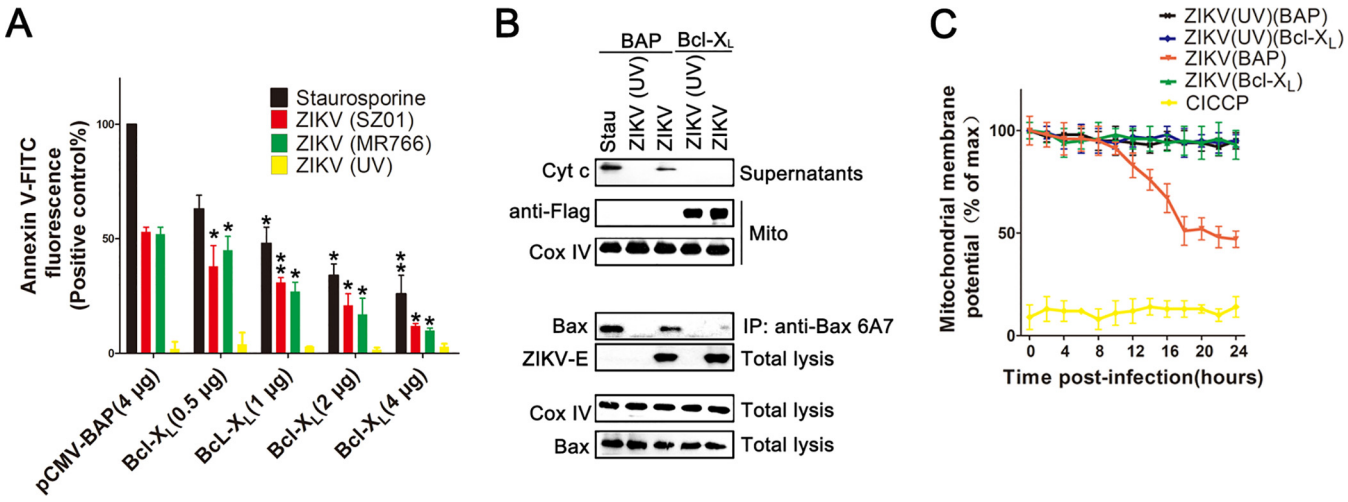

FIG 7 Inhibition of ZIKV infection-induced apoptosis in SY5Y cells by Bcl-X_L. (A) Analysis of ZIKV infection-induced apoptosis in SY5Y cells overexpressing Bcl-X_L by Annexin V-FITC staining and flow cytometry. Staurosporine, cells treated with 30 nM staurosporine for 12 h. pCMV-BAP (4 μg), SY5Y cells transfected with 4 μg pCMV-BAP which could overexpress bacterial alkaline phosphatase (BAP). (B) Western blot of Cyt c and Bax in cell line with ZIKV infection. SY5Y cells or SY5Y cells overexpressing Bcl-X_L were infected with ZIKV for 24 h, and the cytosolic and mitochondrial fractions were separated. Cell lysates were immunoblotted with antibody to Bax, Cox IV, and ZIKV-E and immunoprecipitated with anti-Bax6A7 antibody. The separated cytosolic fractions were immunoblotted with anti-Cyt c antibody, while the mitochondrial fractions were immunoblotted with antibody to Flag and Cox IV. BAP: SY5Y cells that overexpress bacterial alkaline phosphatase. Bcl-X_L, SY5Y cells that overexpress Bcl-X_L. (C) Flow cytometry analysis of the inner mitochondrial membrane potential in cells with ZIKV infection. Cells were infected with ZIKV for 24 h, stained with TMRE for 10 min at 37°C, and subjected to flow cytometry analysis. ZIKV (BAP): SY5Y cells that overexpress bacterial alkaline phosphatase. CICCP: SY5Y cells treated with 10 μM carbonyl cyanide *m*-chlorophenyl hydrazine. Data are from three independent experiments, and the results are presented as mean ± SEM. ** indicates a significant difference at *P* values of 0.02 compared to the control; * indicates a significant difference at *P* values of 0.05 compared to the control.

maintained high levels of TMRE fluorescence similar to those of the cells infected with ZIKV (UV), which indicated that preexpressed Bcl-X_L could inhibit the loss of the inner mitochondrial membrane potential induced by ZIKV infection.

ZIKV NS4B localizes to the mitochondria and could induce Bax activation. Since ZIKV infection induces the classic signs of mitochondrial apoptotic pathway, we attempted to determine which viral proteins triggered that process. We measured apoptosis in SY5Y cells transfected with the plasmids that expressed ZIKV proteins (capsid, envelope M, NS1, NS2A, NS2B, NS3, NS4A, NS4B, or NS5). Results showed that NS4B induced cell apoptosis remarkably. The overexpression of viral membrane protein NS4A led to low levels of cell apoptosis (Figure. 8A).

To determine the distribution of ZIKV NS4B, SY5Y cells were transfected with a vector expressing either ZIKV NS4B or BAP with a C-terminal Flag fusion (pCMV-NS4B and pCMV-BAP, respectively). The cytosol and mitochondria fractions of these cells were separated by centrifugation, and equal amounts of proteins were resolved by SDS-PAGE, followed by immunoblotting with the corresponding antibody. As shown in Fig. 8B, in the total cell lysis, both BAP and NS4B could be detected. However, in the mitochondria fraction, only NS4B can be detected, which indicates that NS4B localizes to the mitochondria. A large amount of activated Bax could be precipitated in staurosporine-treated and NS4B-expressing cells, in addition to BAP-expressing cells.

To further assess the ability of NS4B to initiate apoptosis in SY5Y cells, we monitored the release of Cyt c in the separated supernatants of cells expressing NS4B. Results showed that cells with NS4B expression or treated with staurosporine displayed a clear loss of Cyt c from the mitochondria fraction into the cytosol fraction (Fig. 8B). The cell viability and caspase-3 activity were determined in NS4B-expressed cells transfected with siRNA or overexpressed with Bcl-X_L. Cells expressing BAP were used as a negative control. Results showed that NS4B rapidly induced the decrease of cell viability in the siBak-, siCaspase-8-, siCaspase-10-, and siControl-transfected cells, and the loss of cell viability was more than 30% (Fig. 8D). However, the loss of cell viability induced by NS4B was delayed in siBax-, siCaspase-9-, and Bcl-X_L-transfected cells, with

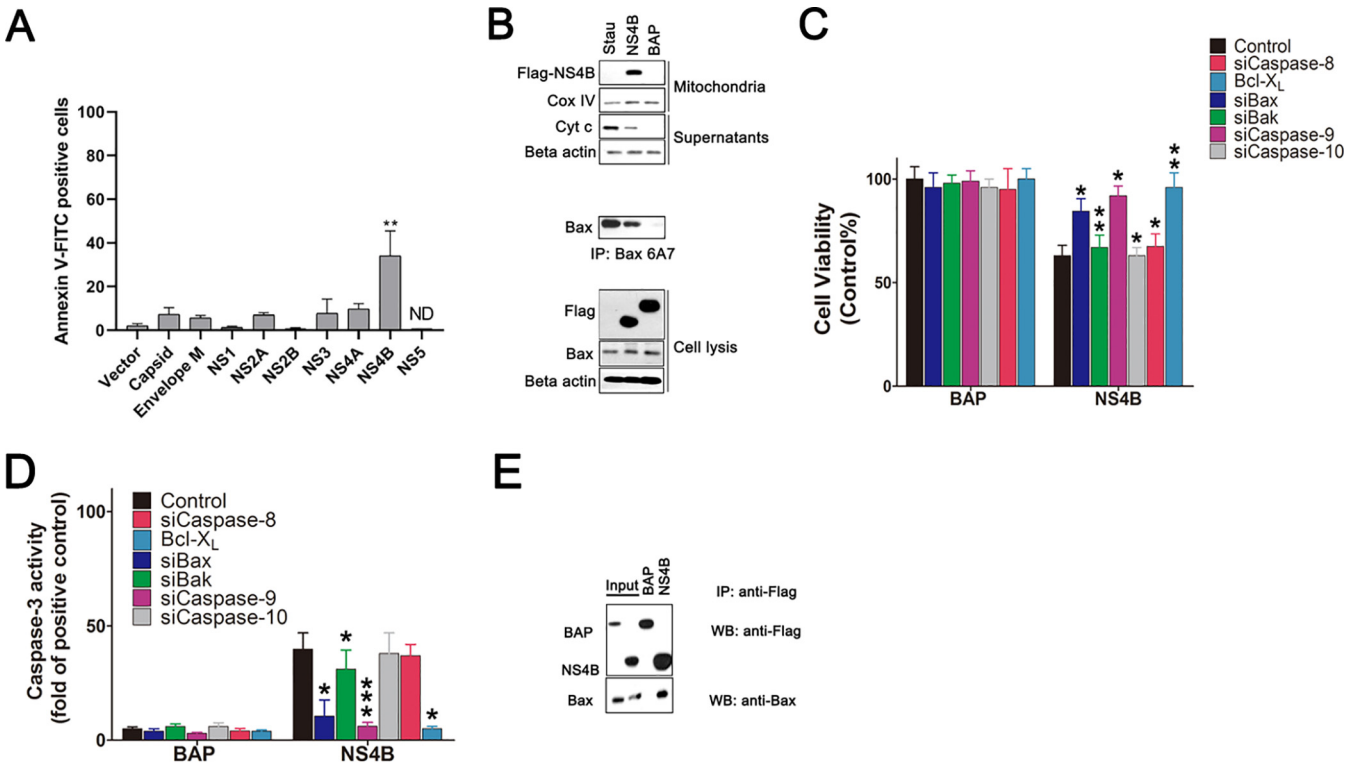

FIG 8 NS4B localizes to the mitochondria and activates the mitochondrial component of the apoptotic cascade. (A) Screening of ZIKV proteins for apoptosis induction. SY5Y cells transfected with vectors that express Flag-tagged NS1, NS2A, NS2B, NS3, NS4A, NS4B, NS5, Capsid, and Envelope M for 24 h. The cells were harvested and stained with Annexin V-FITC. Vector: pCMV-Flag. ND, no data. (B) Western blot of the sublocation of NS4B and activation of Bax. SY5Y cells were transfected with pCMV-NS4B or pCMV-BAP for 24 h or treated with 30 nM staurosporine for 12 h. Cell lysates were immunoblotted with antibody to Bax, beta-actin, and Flag and immunoprecipitated with anti-Bax6A7 antibody. The separated cytosolic fractions were immunoblotted with anti-Cyt c antibody, while the mitochondrial fractions were immunoblotted with antibody to Flag and Cox IV. Stau: staurosporine. (C) Analysis of the impact of NS4B expression on the viability of siRNA-transfected SY5Y cells or SY5Y overexpressing cells. Cells were transfected with the siRNAs as described in Materials and Methods. At 48 h transfection, they were transfected with either pCMV-NS4B or pCMV-BAP for another 48 h and then subjected to cell viability analysis. Control, siControl cells treated with DMSO. (D) Analysis of the impact of NS4B on caspase-3-like activity in cell lysates of siRNA-transfected cells. Caspase-3 activity was determined as described in Materials and Methods. Control, siControl-transfected cells treated with 30 nM staurosporine. (E) Detection of specific interactions between NS4B and cellular Bax in cell lysates by immunoprecipitation assays and Western blot. SY5Y cells were transfected with pCMV-NS4B or pCMV-BAP. At 24 h posttransfection, cell lysates were applied to an anti-Flag immunoaffinity column. After elution with Flag-peptide buffer, the eluted fractions were probed with anti-Flag and anti-BaxNT antibody. Input: cell lysates overexpressed with NS4B or BAP. Data are from three independent experiments, and the results are presented as mean ± SEM. IP, immunoprecipitation. WB, Western blot. ** indicates a significant difference at *P* values of 0.02 compared to the control; * indicates a significant difference at *P* values of 0.05 compared to the control.

about 10% of the loss of cell viability compared to cell death induced in BAP group. NS4B also induced relatively high levels of caspase-3-like activity in cells transfected with siBak, siCaspase-8, siCaspase-10, and siControl, while cells transfected with siBax, siCaspase-9, and pCMV-Bcl-X_L displayed significantly less of active caspase-3 (Fig. 8D).

To determine whether ZIKV NS4B functions by interacting with Bax, we performed a coimmunoprecipitation assay. SY5Y cells transfected with plasmids expressing Flag-tagged NS4B and TAP were lysed and applied to an anti-Flag immunoaffinity column. The Flag-tagged proteins were eluted and confirmed by immunoblotting with anti-Flag and anti-Bax antibody. The results showed that SY5Y cells transfected with pCMV-NS4B-Flag or pCMV-TAP-Flag vector could express NS4B, TAP, and the endogenous Bax. However, the Bax can be detected not only in the eluted NS4B fractions but also in the TAP fractions (Fig. 8E). This means that NS4B interacts directly with Bax. Altogether, ZIKV NS4B could interact with Bax and initiate apoptosis by the release of Cyt c, activation of caspase-3, and the loss of cell viability. The knockdown of Bax and caspase-9 and overexpression of Bcl-X_L could inhibit the caspase-3 activity and the loss of cell viability in NS4B overexpressing cells, which is similar to the phenomenon induced by ZIKV infection.

DISCUSSION

The association between microcephaly in newborns and ZIKV infection has becoming very apparent, based on lines of evidence from human cases and animal studies (10, 34, 35). Microcephaly is probably caused by a depletion of the founder population of radial glia and neural stem cells in the developing brain, through either apoptotic neural progenitor cells death or premature differentiation (28, 36). *In vitro*, ZIKV infection impaired neural progenitor cells proliferation and rapidly induced apoptotic cell death through cleavage of caspases 3, 8, and 9 (18). Therefore, the association between ZIKV infection-induced apoptosis and central nervous system abnormalities at birth would present a valuable model for investigating the mechanisms underlying neurodevelopmental effects of ZIKV infection and exploring candidate therapeutics.

In this study, we have demonstrated that the replication of ZIKV strains SZ01 and MR766 is highly efficient in human neuroblastoma SY5Y cells and that classic mitochondrial apoptosis was induced. The activation and recruitment of Bax from the cytoplasm to mitochondria are indispensable in this apoptotic pathway. Only the Bax was activated, and the outer mitochondrial membrane would be permeabilized and release proapoptogenic factors, such as Cyt c, which then promote the activation of the caspase-3 and caspase-9 that mediate cellular destruction. The mechanism by which this occurs is probably that the overexpressed ZIKV NS4B at the mitochondrial membrane activates the proapoptotic protein Bax.

However, the detailed mechanism of activation of proapoptotic protein Bax by NS4B remains unclear. NS4B localizes to mitochondria and triggers the exposure of the Bax N-terminal transmembrane domain, resulting in the disruption of the mitochondrial transmembrane potential and Cyt c release. Alternatively, NS4B may create a mitochondrion whose environment is favorable for the interaction and oligomerization of Bax protein and other molecules from the mitochondria. The existence of NS4B may lead to enhanced Bax activity when Bax "inhibitor" molecules in the cells are sequestered.

The activation of Bax inducing alterations in the mitochondria is currently controversial. Bax has been shown to form channels in synthetic membranes and may even create very high conductance channels under some circumstances (26). It is possible that Bax creates pores in the mitochondria outer membrane which are large enough to allow the escape of Cyt c (37). Alternatively, Bax might indirectly alter the permeability of the outer membrane through interactions with other proteins (38). Further experimentation is needed to verify any of these possibilities.

As a member of the genus *Flavivirus* and the family *Flaviviridae* (39), ZIKV is closely related to West Nile virus (WNV), Dengue virus (DENV), Japanese encephalitis virus (JEV), and other human flaviviruses (40, 41). Infection with those flaviviruses has been shown to activate several signaling pathways such as endoplasmic reticulum (ER)-stress and AKT/PI3K pathway, resulting in activation or suppression of apoptosis in virus-infected cells (42). The nuclear localization of DENV capsid protein is required for its interaction with Fas death domain associated protein xx (DAXX) and the induction of apoptosis (43). NS2A is involved in WNV-induced apoptosis and pathogenesis. The protease activity of NS3 in JEV and DENV induces apoptosis through the activation of caspase-3 or caspase-8. NS2B, a cofactor of NS3, is required for the induction of NS3-induced apoptosis (44–46). Based on current research, the involvement of Bax in flavivirus-induced apoptosis is more specific to ZIKV. However, further investigation is needed to verify any of these possibilities.

This report presents new insights into understanding the interplay between apoptosis and ZIKV infection, which is different from apoptosis induced by JEV, DENV, and WNV infection. SY5Y cells lacking Bax expression showed resistance to ZIKV infection-induced apoptosis, which provides the evidence that ZIKV induces cell apoptosis by modulating Bax activation and reveals important clues regarding the mechanism of Cyt c release and mitochondria permeabilization during ZIKV infection. Furthermore, the robust apoptosis phenotype displayed by mice (Ifnar1$^{-/-}$) spleens and fetal brains offers a useful model for testing candidate therapeutics and for investigating genetic

TABLE 1 Reagents and antibodies used in this manuscript[a]

Antibodies/reagents	Source	Identifier	Working dilutions
Caspase-3 antibody	CST	#9662S	1:2,000 (WB)
Cleaved-caspase-3 antibody	CST	#9661	1:500 (IF); 1:2,000 (WB)
Caspase-8 antibody	Abcam	Ab108333	1:2,000 (WB)
Caspase-9 antibody	Abcam	Ab32539	1:2,000 (WB)
Caspase-10 antibody	Abcam	Ab32155	1:2,000 (WB)
Bcl-X_L antibody	CST	#2764	1:2,000 (WB)
BSA antibody	CST	#66271	1:2,000 (WB)
Cyt c antibody	CST	#11940	1:2,000 (WB)
Flag antibody	Santa Cruz	Ab205606	1:4,000 (WB)
Bak antibody	Santa Cruz	SC518110	1:500 (WB)
Bak (Ab-1, clone TC-100) antibody	Merck	AM03	1:500 (F)
Beta-actin antibody	Santa Cruz	SC8432	1:4,000 (WB)
Cox IV antibody	CST	#4850	1:200
Bax (6A7) antibody	Santa Cruz	SC23959	1:200 (IP); 1:500 (F)
HRP-conjugated anti-rabbit IgG	Santa Cruz	SC2004	1:1,000 (WB)
FITC-conjugated anti-rabbit IgG	Santa Cruz	SC2012	1:1,000 (IF)
FITC-conjugated anti-mouse IgG	ZSGB-BIO	ZF-0312	1:1,000 (IF)
HRP-conjugated anti-mouse IgG	Santa Cruz	SC2010	1:1,000 (WB)
zLEHD.Fmk	Beyotime	C1202	15 μM
zDEVD.Fmk	Beyotime	C1206	25 μM
Staurosporine	Beyotime	S1882	30 nM
CICCP	Sigma-Aldrich	#555-60-2	10 μM

[a]WB: western blot; IF: immunofluorescence; F: Flow cytometry.

or other biological factors that may confer increased susceptibility or resistance to the neurodevelopmental defects due to ZIKV infection.

MATERIALS AND METHODS

Cells and viruses. SY5Y and Vero cells were propagated and maintained in double modified Eagle's medium (DMEM) supplemented with antibiotics (penicillin and streptomycin) and 10% fetal bovine serum (Invitrogen), at 37°C in the presence of 5% CO_2. The ZIKV strains SZ01 and MR766 kindly provided by Bi Yuhai and Li Shihua (Institute of Microbiology, Chinese Academy of Sciences, Beijing, People's Republic of China) were propagated and purified as described by Prestwood et al. (47). The ZIKV (UV) is a mutant of ZIKV (MR766) derived by treatment with UV light. Briefly, 200 μl of ZIKV preparations containing 2.5% fetal calf serum (FCS) was exposed to UV light of a laminar flow for up to 60 min. Cells were infected with ZIKV at a multiplicity of infection (MOI = 1). After adsorption for 1 h at 4°C, the cells were washed twice with phosphate-buffered saline (PBS) and cultured in DMEM containing 2% calf serum at 37°C in the presence of 5% CO_2.

Virus titer determination. To determine virus titers, Vero cells were plated into 96-well dishes and infected with the serially diluted ZIKV. After incubation for 45 min at 37°C, the virus suspension was replaced with DMEM containing 2% fetal bovine serum. The cultures were incubated at 37°C for 3 days, and plates with cytopathic effects were counted. Virus titers were determined by the Reed-Muench method. Virus titer values presented are means and standard deviations (SD) based on three independent experiments.

Ethics statement. This study was performed in strict accordance with the recommendations in the guide for the care and use of laboratory animals of the Institute of Microbiology, Chinese Academy of Sciences (IMCAS) Ethics Committee, and all experiments conform to the relevant regulatory standards. The experiments and protocol were approved by the Committee on the Ethics of Animal Experiments of IMCAS. All animal experiments were conducted under isoflurane anesthesia to minimize animal suffering. Studies with ZIKV were conducted in a biosafety level 2 (BSL2) lab.

Mouse experiments. Type I IFN receptor α chain null mice (Ifnar1$^{-/-}$) were backcrossed onto a C57BL/6 background (48). Ifnar1$^{-/-}$ mice were purchased from Jackson Laboratories (USA) and were bred in a specific-pathogen-free facility at Institute of Microbiology, Chinese Academy of Sciences. Seven-week-old Ifnar1$^{-/-}$ mice were intraperitoneally (i.p.) injected with a total dose of 10^3 PFU ZIKV (n = 10 for each group). At 5 days postinfection, the mice were euthanized and the spleen was harvested for immunofluorescence analyses. Pregnant Ifnar1$^{-/-}$ mice were inoculated with 10^3 PFU of ZIKV via a subcutaneous route. After 7 days, the brains of fetal mice were collected for immunofluorescence analysis.

Reagents and antibodies. The protease inhibitor cocktail, staurosporine, 4′,6-diamidino-2-phenylindole (DAPI), and TMRE were obtained from Sigma-Aldrich (Missouri). DMSO, bis-maleimidohexane (BMH), and Lipofectamine 3000 transfection reagent were obtained from Invitrogen (USA). ZIKV-specific polyclonal antibody was produced from rabbit immunized with ZIKV-E protein. ZIKV-specific monoclonal antibody was obtained from Dr. Wang (Institute of Microbiology, Chinese Academy of Sciences, Beijing,

TABLE 2 Sequences of siRNAs used in this paper

siRNA	Sequence
siControl	UUCUUCGAACGUGUCACGUUU
siBax	GGUCACCUUACCUCUGCAAUU
siBak	GGAGCUGCAGAGGAUGAUUUU
siCaspase-8	AACCUCGGGGAUACUGUCUGA
siCaspase-9	UUGCGGCGUCGCUUCUCCUC
siCaspase-10	UUCUGACCCAUGGGAGAUUU

People's Republic of China). Other antibodies and reagents are listed in Table 1. Caspase-3 activity assay kit, caspase-9 activity assay kit, and Annexin V-FITC were obtained from Biyotime, China.

Cell viability, mitochondrial membrane potential, and caspase-3 activity assays. Cell viability was analyzed as described by using CCK-8 kit (31). CCK-8 reagent was added into each dish, incubated for 2 h, and measured at 450 nm and 600 nm using microplate reader. To detect cell apoptosis, the cells were harvested and resuspended in Annexin V binding buffer at a concentration of 1×10^6 cells/ml. The cells were mixed with Annexin V-FITC and then incubated for 15 min at room temperature in the dark. The fluorescence signals were detected by BD FACSCalibur (Becton, Dickinson) and data were quantified using the Cellquest software (Becton, Dickinson).

Mitochondrial membrane potential was assayed by staining the cells with TMRE (Molecular Probes). The cells were stained by incubating them in a medium buffer containing 0.2 μM TMRE for 20 min at 37°C. After washing thrice with PBS, TMRE fluorescence was detected by flow cytometry.

The activity of caspases-3 and caspase-9 was measured with the Ac-DEVD-pNA and Ac-LEHD-pNA assay kit according to the manufacturer's instructions. Briefly, 200 μl of Ac-DEVD-pNA reagent were added to each well containing 40 μl aliquots of cell supernatants, mixed using a plate shaker at 300 to 500 rpm, and incubated at room temperature for 0.5 h. The luminescence of each sample was measured in a fluorescent microplate reader (Bio-Rad, CA, USA) at the excitation/emission wavelengths of 400/505 nm.

Mitochondria isolation and Bax cross-linking. Mitochondrial fractions were prepared as before (49, 50). In brief, cells were lysed and centrifuged at 2,000 $\times$ *g* for 10 min, and pellet was resuspended in cold mitochondria isolation buffer for 10 min and centrifuged at 3,000 $\times$ *g* for 5 min to pellet the unlysed cells and nuclei. The supernatant was further centrifuged at 14,000 $\times$ *g* for 20 min to obtain the mitochondria pellet. The mitochondria fraction was directly used for other experiments.

For Bax cross-linking, the mitochondria were resuspended in PBS buffer (pH 7.2) and subjected to cross-linking using 0.2 mM BMH for 2 h at 4°C. The reaction was stopped by adding quenching solution and stored at −20°C for later analysis by Western blotting.

RNA interference experiments. SY5Y cells were plated in culture dishes and allowed to grow for 24 h to approximately 90% confluence. A mixture of Opti-MEM medium and Lipofectamine 3000 was incubated for 5 min at room temperature before adding 50 nM siRNA (siRNA sequences are listed in Table 2) and then incubated for 10 min at room temperature. This mixture including siRNA or recombinant plasmid was then added to the well. Twenty-four hours after transfection, the medium was changed and analyses were performed at the indicated time after transfection. Gene silencing or protein expression was verified by detecting proteins by Western blotting after transient transfection of SY5Y cells with siRNA.

Immunofluorescence, immunoprecipitation, and Western blot. For cells immunofluorescence, cells were stained using mitotracker red (50 nM) and grown on coverslips for 15 min. The cells were then fixed with 4% paraformaldehyde for 30 min and permeabilized with 0.2% NP-40 for 15 min. For ZIKV staining, we used a fluorescein isothiocyanate (FITC) conjugated human monoclonal antibody or mouse monoclonal antibody against ZIKV protein E. For cleaved-caspase-3 staining, caspase-3 monoclonal antibody was used. For activated Bax staining, Bax (6A7) monoclonal antibody was used. After three washes with PBS, immunofluorescence was examined under an inverted fluorescence or a confocal laser scanning microscope.

For tissues immunofluorescence, spleens and fetal brain were fixed in 10% neutral phosphate-buffered formalin, routinely processed, and sectioned at 6 μm. Frozen tissue sections were air-dried for 10 min at room temperature before fixing with ice cold acetone for 10 min. The sections were washed by PBS 3 times and blocked with blocking buffer (1% BSA, 0.3% Triton, 1$\times$ PBS) at 37°C for 30 min. The sections were then incubated with the primary antibody (caspase-3 or Bax6A7) at 4°C overnight. After rinsing with PBS, secondary antibody was applied for 1 h at 37°C. The sections were then washed with PBS and counterstained for nuclei using DAPI following the manufacturer's instructions.

Immunoprecipitation was performed as described before (32). In short, anti-Bax6A7 or anti-Flag monoclonal antibody was immobilized on agarose beads. After washing three times with PBS and once with lysis buffer, the beads were incubated with cell lysate overnight at 4°C with gentle rocking. After washing with lysis buffer and PBS, the incubated beads were boiled and proteins in the supernatant were collected and subjected to Western blotting.

For Western blotting, cells were extracted with radioimmunoprecipitation assay (RIPA) buffer with protease inhibitor, incubated for 30 min on ice, and centrifuged at 12,000 $\times$ *g* for 10 min at 4°C, and the supernatants were collected. Equal amounts of protein (50 μg) were heat-denatured in sample-loading

buffer and separated by SDS–PAGE (10% polyacrylamide, 0.1% SDS). Proteins were then blotted with the following antibodies: monoclonal anti-Bax diluted at 1:2,000, anti-Flag diluted at 1:2,000, anti-β-actin diluted at 1:4,000, anti-CoxIV diluted at 1:2,000, anti-ZIKV, caspase-8, -9, and -10, cytochrome *c*, and Bak diluted at 1:1,000.

Plasmid construction and protein expression. To create expression vectors that express Flag-tagged NS1, NS2A, NS2B, NS3, NS4A, NS4B, NS5, capsid, envelope M, and BAP, all of those genes were chemically synthesized and ligated to the HindIII and SalI sites of the pCMV-C-Flag vector. The full-length human cDNA for Bcl-X_L was cloned and ligated to the restriction site of the pcDNA3.1-Flag plasmid after digesting with PstI and SalI. The recombinant plasmid was then transfected into SY5Y cells by using Lipofectamine 3000 according to the manufacturer's instructions. The expression of Bcl-X_L-Flag in transfectants was confirmed by Western blotting. Recombinant Bax with a Flag tag was expressed and purified as described before (49).

Statistical analysis. Data were subjected to one-way analysis of variance with factors of treatments and expressed as means plus or minus standard deviation (SD). Comparisons between any two groups were performed by unpaired Student's *t* tests.

ACKNOWLEDGMENTS

This work was supported by the National Natural Science Foundation of China (grant 32060039), grants from the Program Funded by University for Young Scientific and Technological Backbone (2017XQC-2), and the research project of high-level talents (NDYB2016-12).

We are grateful to Paul Chu, Guest Professor of the Institute of Microbiology, Chinese Academy of Sciences, for his kind help during the preparation of the manuscript. We also thank Weihua Zhuang and Fulian Liao, Institute of Microbiology, CAS, for help with experiments.

REFERENCES

1. Dick GW, Kitchen SF, Haddow AJ. 1952. Zika virus. I. Isolations and serological specificity. Trans R Soc Trop Med Hyg 46:509–520. https://doi.org/10.1016/0035-9203(52)90042-4.
2. Salehuddin AR, Haslan H, Mamikutty N, Zaidun NH, Azmi MF, Senin MM, Syed Ahmad Fuad SB, Thent ZC. 2017. Zika virus infection and its emerging trends in Southeast Asia. Asian Pac J Trop Med 10:211–219. https://doi.org/10.1016/j.apjtm.2017.03.002.
3. Hancock WT, Marfel M, Bel M. 2014. Zika virus, French Polynesia, South Pacific, 2013. Emerg Infect Dis 20:1960. https://doi.org/10.3201/eid2011.141380.
4. Hennessey M, Fischer M, Staples JE. 2016. Zika virus spreads to new areas – region of the Americas, May 2015–January 2016. Mmwr Morb Mortal Wkly Rep 65:55–58. https://doi.org/10.15585/mmwr.mm6503e1.
5. Kleber de Oliveira W, Cortez-Escalante J, De Oliveira WT, do Carmo GM, Henriques CM, Coelho GE, Araujo de Franca GV. 2016. Increase in reported prevalence of microcephaly in infants born to women living in areas with confirmed Zika virus transmission during the first trimester of pregnancy - Brazil, 2015. Mmwr Morb Mortal Wkly Rep 65:242–247. https://doi.org/10.15585/mmwr.mm6509e2.
6. Dos Santos Oliveira SJG, Dos Reis CL, Cipolotti R, Gurgel RQ, Santos VS, Martins-Filho PRS. 2017. Anxiety, depression, and quality of life in mothers of newborns with microcephaly and presumed congenital Zika virus infection: a follow-up study during the first year after birth. Arch Womens Ment Health 20:473–475. https://doi.org/10.1007/s00737-017-0724-y.
7. Rather IA, Lone JB, Bajpai VK, Park YH. 2017. Zika virus infection during pregnancy and congenital abnormalities. Front Microbiol 8:581. https://doi.org/10.3389/fmicb.2017.00581.
8. Schuler-Faccini L, Ribeiro EM, Feitosa IML, Horovitz DDG, Cavalcanti DP, Pessoa A, Doriqui MJR, Neri JI, Neto JMD, Wanderley HYC, Cernach M, El-Husny AS, Pone MVS, Serao CLC, Sanseverino MTV, Embry B, Brazilian Medical Genetics Society–Zika Embryopathy Task Force. 2016. Possible association between Zika virus infection and microcephaly - Brazil, 2015. MMWR Morb Mortal Wkly Rep 65:59–62. https://doi.org/10.15585/mmwr.mm6503e2.
9. Kasprzykowski JI, Fukutani KF, Fabio H, Fukutani ER, Costa LC, Andrade BB, Queiroz ATL. 2020. A recursive sub-typing screening surveillance system detects the arising of the ZIKV African lineage in Brazil: is there risk of a new epidemic? Int J Infect Dis 96:579–581 https://doi.org/10.1016/j.ijid.2020.05.090.
10. Cauchemez S, Besnard M, Bompard P, Dub T, Guillemette-Artur P, Eyrolle-Guignot D, Salje H, Van Kerkhove MD, Abadie V, Garel C, Fontanet A, Mallet HP. 2016. Association between Zika virus and microcephaly in French Polynesia, 2013–15: a retrospective study. Lancet 387:2125–2132. https://doi.org/10.1016/S0140-6736(16)00651-6.
11. Petersen EE, Staples JE, Meaney-Delman D, Fischer M, Ellington SR, Callaghan WM, Jamieson DJ. 2016. Interim guidelines for pregnant women during a Zika virus outbreak–United States, 2016. Mmwr Morb Mortal Wkly Rep 65:30–33. https://doi.org/10.15585/mmwr.mm6502e1.
12. Olagnier D, Muscolini M, Coyne CB, Diamond MS, Hiscott J. 2016. Mechanisms of Zika virus infection and neuropathogenesis. DNA Cell Biol 35:367–372. https://doi.org/10.1089/dna.2016.3404.
13. Nowakowski TJ, Pollen AA, Di Lullo E, Sandoval-Espinosa C, Bershteyn M, Kriegstein AR. 2016. Expression analysis highlights AXL as a candidate Zika virus entry receptor in neural stem cells. Cell Stem Cell 18:591–596. https://doi.org/10.1016/j.stem.2016.03.012.
14. Hamel R, Dejarnac O, Wichit S, Ekchariyawat P, Neyret A, Luplertlop N, Perera-Lecoin M, Surasombatpattana P, Talignani L, Thomas F, Cao-Lormeau VM, Choumet V, Briant L, Despres P, Amara A, Yssel H, Misse D. 2015. Biology of Zika virus infection in human skin cells. J Virol 89:8880–8896. https://doi.org/10.1128/JVI.00354-15.
15. Li C, Xu D, Ye Q, Hong S, Jiang Y, Liu X, Zhang N, Shi L, Qin CF, Xu Z. 2016. Zika virus disrupts neural progenitor development and leads to microcephaly in mice. Cell Stem Cell 19:672. https://doi.org/10.1016/j.stem.2016.10.017.
16. Tang H, Hammack C, Ogden SC, Wen Z, Qian X, Li Y, Yao B, Shin J, Zhang F, Lee EM, Christian KM, Didier RA, Jin P, Song H, Ming GL. 2016. Zika virus infects human cortical neural progenitors and attenuates their growth. Cell Stem Cell 18:587–590. https://doi.org/10.1016/j.stem.2016.02.016.
17. Huang WC, Abraham R, Shim BS, Choe H, Page DT. 2016. Zika virus infection during the period of maximal brain growth causes microcephaly and corticospinal neuron apoptosis in wild type mice. Sci Rep 6:34793. https://doi.org/10.1038/srep34793.
18. Souza BS, Sampaio GL, Pereira CS, Campos GS, Sardi SI, Freitas LA, Figueira CP, Paredes BD, Nonaka CK, Azevedo CM, Rocha VP, Bandeira AC, Mendez-Otero R, Dos Santos RR, Soares MB. 2016. Zika virus infection induces mitosis abnormalities and apoptotic cell death of human neural progenitor cells. Sci Rep 6:39775. https://doi.org/10.1038/srep39775.
19. Li H, Zhu H, Xu CJ, Yuan J. 1998. Cleavage of BID by caspase 8 mediates the mitochondrial damage in the Fas pathway of apoptosis. Cell 94:491–501. https://doi.org/10.1016/s0092-8674(00)81590-1.

20. Rokhlin OW, Glover RA, Cohen MB. 1998. Fas-mediated apoptosis in human prostatic carcinoma cell lines occurs via activation of caspase-8 and caspase-7. Cancer Res 58:5870–5875.
21. Green DR, Reed JC. 1998. Mitochondria and apoptosis. Science 281:1309–1312. https://doi.org/10.1126/science.281.5381.1309.
22. Brenner C, Kroemer G. 2000. Apoptosis. Mitochondria–the death signal integrators. Science 289:1150–1151. https://doi.org/10.1126/science.289.5482.1150.
23. Dewson G, Kluck RM. 2009. Mechanisms by which Bak and Bax permeabilise mitochondria during apoptosis. J Cell Sci 122:2801–2808. https://doi.org/10.1242/jcs.038166.
24. Wei MC, Zong WX, Cheng EH, Lindsten T, Panoutsakopoulou V, Ross AJ, Roth KA, MacGregor GR, Thompson CB, Korsmeyer SJ. 2001. Proapoptotic BAX and BAK: a requisite gateway to mitochondrial dysfunction and death. Science 292:727–730. https://doi.org/10.1126/science.1059108.
25. Zhou L, Chang DC. 2008. Dynamics and structure of the Bax-Bak complex responsible for releasing mitochondrial proteins during apoptosis. J Cell Sci 121:2186–2196. https://doi.org/10.1242/jcs.024703.
26. Czabotar PE, Westphal D, Dewson G, Ma S, Hockings C, Fairlie WD, Lee EF, Yao SG, Robin AY, Smith BJ, Huang DCS, Kluck RM, Adams JM, Colman PM. 2013. Bax crystal structures reveal how BH3 domains activate Bax and nucleate its oligomerization to induce apoptosis. Cell 152:519–531. https://doi.org/10.1016/j.cell.2012.12.031.
27. Degenhardt K, Sundararajan R, Lindsten T, Thompson C, White E. 2002. Bax and Bak independently promote cytochrome C release from mitochondria. J Biol Chem 277:14127–14134. https://doi.org/10.1074/jbc.M109939200.
28. Frumence E, Roche M, Krejbich-Trotot P, El-Kalamouni C, Nativel B, Rondeau P, Misse D, Gadea G, Viranaicken W, Despres P. 2016. The South Pacific epidemic strain of Zika virus replicates efficiently in human epithelial A549 cells leading to IFN-beta production and apoptosis induction. Virology 493:217–226. https://doi.org/10.1016/j.virol.2016.03.006.
29. Ihrlund LS, Hernlund E, Viktorsson K, Panaretakis T, Barna G, Sabapathy K, Linder S, Shoshan MC. 2006. Two distinct steps of Bak regulation during apoptotic stress signaling: different roles of MEKK1 and JNK1. Exp Cell Res 312:1581–1589. https://doi.org/10.1016/j.yexcr.2006.01.023.
30. Hanson RL, Porter JR, Batchelor E. 2019. Protein stability of p53 targets determines their temporal expression dynamics in response to p53 pulsing. J Cell Biol 218:1282–1297. https://doi.org/10.1083/jcb.201803063.
31. Sarosiek KA, Chi X, Bachman JA, Sims JJ, Montero J, Patel L, Flanagan A, Andrews DW, Sorger P, Letai A. 2013. BID preferentially activates BAK while BIM preferentially activates BAX, affecting chemotherapy response. Mol Cell 51:751–765. https://doi.org/10.1016/j.molcel.2013.08.048.
32. Cong H, Du N, Yang Y, Song L, Zhang W, Tien P. 2016. Enterovirus 71 2b induces cell apoptosis by directly inducing the conformational activation of the proapoptotic protein Bax. J Virol 90:9862–9877. https://doi.org/10.1128/JVI.01499-16.
33. Minn AJ, Kettlun CS, Liang H, Kelekar A, Vander Heiden MG, Chang BS, Fesik SW, Fill M, Thompson CB. 1999. Bcl-xL regulates apoptosis by heterodimerization-dependent and -independent mechanisms. EMBO J 18:632–643. https://doi.org/10.1093/emboj/18.3.632.
34. Brasil P, Pereira JP, Jr, Moreira ME, Ribeiro Nogueira RM, Damasceno L, Wakimoto M, Rabello RS, Valderramos SG, Halai UA, Salles TS, Zin AA, Horovitz D, Daltro P, Boechat M, Raja Gabaglia C, Carvalho de Sequeira P, Pilotto JH, Medialdea-Carrera R, Cotrim da Cunha D, Abreu de Carvalho LM, Pone M, Machado Siqueira A, Calvet GA, Rodrigues Baiao AE, Neves ES, Nassar de Carvalho PR, Hasue RH, Marschik PB, Einspieler C, Janzen C, Cherry JD, Bispo de Filippis AM, Nielsen-Saines K. 2016. Zika virus infection in pregnant women in Rio de Janeiro. N Engl J Med 375:2321–2334. https://doi.org/10.1056/NEJMoa1602412.
35. Miner JJ, Cao B, Govero J, Smith AM, Fernandez E, Cabrera OH, Garber C, Noll M, Klein RS, Noguchi KK, Mysorekar IU, Diamond MS. 2016. Zika virus infection during pregnancy in mice causes placental damage and fetal demise. Cell 165:1081–1091. https://doi.org/10.1016/j.cell.2016.05.008.
36. Barkovich AJ, Guerrini R, Kuzniecky RI, Jackson GD, Dobyns WB. 2012. A developmental and genetic classification for malformations of cortical development: update 2012. Brain 135:1348–1369. https://doi.org/10.1093/brain/aws019.
37. Green DR, Chipuk JE. 2008. Apoptosis: stabbed in the BAX. Nature 455:1047–1049. https://doi.org/10.1038/4551047a.
38. Belzacq AS, Vieira HL, Verrier F, Vandecasteele G, Cohen I, Prevost MC, Larquet E, Pariselli F, Petit PX, Kahn A, Rizzuto R, Brenner C, Kroemer G. 2003. Bcl-2 and Bax modulate adenine nucleotide translocase activity. Cancer Res 63:541–546.
39. Hayes EB. 2009. Zika virus outside Africa. Emerg Infect Dis 15:1347–1350. https://doi.org/10.3201/eid1509.090442.
40. Lazear HM, Govero J, Smith AM, Platt DJ, Fernandez E, Miner JJ, Diamond MS. 2016. A mouse model of Zika virus pathogenesis. Cell Host Microbe 19:720–730. https://doi.org/10.1016/j.chom.2016.03.010.
41. Saiz JC, Vazquez-Calvo A, Blazquez AB, Merino-Ramos T, Escribano-Romero E, Martin-Acebes MA. 2016. Zika virus: the latest newcomer. Front Microbiol 7:496. https://doi.org/10.3389/fmicb.2016.00496.
42. Okamoto T, Suzuki T, Kusakabe S, Tokunaga M, Hirano J, Miyata Y, Matsuura Y. 2017. Regulation of apoptosis during flavivirus infection. Viruses-Basel 9:243. https://doi.org/10.3390/v9090243.
43. Netsawang J, Noisakran S, Puttikhunt C, Kasinrerk W, Wongwiwat W, Malasit P, Yenchitsomanus PT, Limjindaporn T. 2010. Nuclear localization of dengue virus capsid protein is required for DAXX interaction and apoptosis. Virus Res 147:275–283. https://doi.org/10.1016/j.virusres.2009.11.012.
44. Yang TC, Shiu SL, Chuang PH, Lin YJ, Wan L, Lan YC, Lin CW. 2009. Japanese encephalitis virus NS2B-NS3 protease induces caspase 3 activation and mitochondria-mediated apoptosis in human medulloblastoma cells. Virus Res 143:77–85. https://doi.org/10.1016/j.virusres.2009.03.007.
45. Shafee N, AbuBakar S. 2003. Dengue virus type 2 NS3 protease and NS2B-NS3 protease precursor induce apoptosis. J Gen Virol 84:2191–2195. https://doi.org/10.1099/vir.0.19022-0.
46. Ramanathan MP, Chambers JA, Pankhong P, Chattergoon M, Attatippaholkun W, Dang KS, Shah N, Weiner DB. 2006. Host cell killing by the West Nile Virus NS2B-NS3 proteolytic complex: NS3 alone is sufficient to recruit caspase-8-based apoptotic pathway. Virology 345:56–72. https://doi.org/10.1016/j.virol.2005.08.043.
47. Prestwood TR, Prigozhin DM, Sharar KL, Zellweger RM, Shresta S. 2008. A mouse-passaged dengue virus strain with reduced affinity for heparan sulfate causes severe disease in mice by establishing increased systemic viral loads. J Virol 82:8411–8421. https://doi.org/10.1128/JVI.00611-08.
48. Hwang SY, Hertzog PJ, Holland KA, Sumarsono SH, Tymms MJ, Hamilton JA, Whitty G, Bertoncello I, Kola I. 1995. A null mutation in the gene encoding a type I interferon receptor component eliminates antiproliferative and antiviral responses to interferons alpha and beta and alters macrophage responses. Proc Natl Acad Sci U S A 92:11284–11288. https://doi.org/10.1073/pnas.92.24.11284.
49. Jurgensmeier JM, Xie Z, Deveraux Q, Ellerby L, Bredesen D, Reed JC. 1998. Bax directly induces release of cytochrome c from isolated mitochondria. Proc Natl Acad Sci U S A 95:4997–5002. https://doi.org/10.1073/pnas.95.9.4997.
50. Sun FC, Wei S, Li CW, Chang YS, Chao CC, Lai YK. 2006. Localization of GRP78 to mitochondria under the unfolded protein response. Biochem J 396:31–39. https://doi.org/10.1042/BJ20051916.